Am J Transl Res 2020;12(9):5511-5524
www.ajtr.org /ISSN:1943-8141/AJTR0112964

Original Article

Antitumor properties of arsenic trioxide-loaded CalliSpheres® microspheres by transarterial chemoembolization in VX2 liver tumor rabbits: suppression of tumor growth, angiogenesis, and metastasis and elongation of survival

Xuhua Duan*, Hao Li*, Xinwei Han, Jianzhuang Ren, Fengyao Li, Shuguang Ju, Manzhou Wang, Wenhui Wang

*Department of Interventional Radiology, The First Affiliated Hospital, Zhengzhou University, Zhengzhou, P. R. China. *Equal contributors.*

Received April 21, 2020; Accepted August 7, 2020; Epub September 15, 2020; Published September 30, 2020

Abstract: This study aimed to investigate the antitumor effect of arsenic trioxide (ATO)-loaded CalliSpheres® microspheres (CSM) by transarterial chemoembolization (TACE) in rabbits with VX2 liver tumors. A total of 120 VX2 liver tumor rabbits were randomized into four groups (N = 30 for each group), which received ATO-loaded CSM by TACE (CSM-ATO group), ATO by conventional TACE (cTACE-ATO group), transcatheter arterial embolization using CSM (TAE-CSM group), and saline arterial injection (control group). Five rabbits in each group were sacrificed at 12 h, 3 d, 7 d and 14 d, and then tumor proliferation, apoptosis, and angiogenesis/epithelial-mesenchymal transition (EMT) markers were detected. Tumor volume, metastasis status and ascites were assessed at 14 d. Ten rabbits in each group were observed until death for accumulating survival calculation. Tumor volume and ascites were decreased in the CSM-ATO group compared to the cTACE-ATO and TAE-CSM groups. Pulmonary, abdominal wall and omentum metastases were reduced while accumulating survival was increased in the CSM-ATO group compared to the TAE-CSM group. However, no difference in metastasis foci or survival between the CSM-ATO and cTACE-ATO groups was discovered. Meanwhile, tumor apoptosis was promoted while proliferation was suppressed in the CSM-ATO group compared to the cTACE-ATO and TAE-CSM groups. Additionally, HIF-1α, VEGF and microvessel density were decreased in the CSM-ATO group compared to the cTACE-ATO and TAE-CSM groups. Additionally, twist, N-cadherin, vimentin and MMP-9 were reduced while E-cadherin was enhanced in the CSM-ATO group compared to the cTACE-ATO and TAE-CSM groups. In conclusion, ATO-loaded CSM by TACE suppressed tumor growth, angiogenesis, and metastasis and elongated survival in VX2 liver tumor rabbits.

Keywords: Arsenic trioxide, CalliSpheres® microspheres, drug-eluting beads-transarterial chemoembolization, hepatocellular carcinoma, tumor progression

Introduction

Hepatocellular carcinoma (HCC), the predominant type of liver cancer, is one of the major global health problems and caused over 0.84 million newly diagnosed cases and 0.78 million deaths in 2018 [1]. Current treatment for patients with HCC mainly includes surgical resection, orthotopic liver transplantation, ablative techniques, transarterial chemoembolization (TACE), transarterial radioembolization, stereotactic body radiation therapy and systemic chemotherapy, among which TACE is recommended as the first-line therapy for patients with intermediate stage HCC [2, 3]. Conventional TACE (cTACE) is performed by delivering lipiodol emulsified chemotherapy agent, followed by particle embolization [3]. Despite the efficiency of cTACE in inducing tumor necrosis and apoptosis, it is still characterized by relatively high systematic toxicity and abrupt drug delivery [3, 4]. As one of the solutions to improve cTACE, drug-eluting beads (DEB)-TACE uses microspheres as the drug carrier and embolization agent to provide elevated tolerance and more stable drug release, thus improving the

treatment effect in patients with HCC [5, 6]. The commonly used drugs in DEB-TACE treatment include doxorubicin and irinotecan, which have greatly improved the survival of patients with HCC; however, the idealized prognosis of patients with HCC is far from being reached [2, 7]. Therefore, searching for potential anticancer agents by DEB-TACE treatment with eminent treatment efficacy might improve the prognosis of patients with HCC who receive DEB-TACE treatment.

Arsenic trioxide (ATO), an inorganic compound with anticancer properties, has been approved to treat acute promyelocytic leukemia by the Food and Drug Administration since 2000 [8]. For solid tumors (including HCC), ATO has been reported to have a suppressive effect on tumor progression. For example, an interesting study revealed that ATO suppresses tumorigenesis and distant metastasis in a mouse liver cancer model and inhibits cancer stem cell-associated traits by targeting the serum response factor/minichromosome maintenance protein 7 complex in HCC cells [9]. Additionally, another previous study illustrated that the administration of ATO induces mitochondrial apoptosis by inhibiting the phosphorylation of signal transducer and activator of transcription 3 (STAT3) in the HCC cell line Bel-7404 [10]. Despite the benefit of ATO with antitumor properties in HCC, the hypertoxicity of ATO limits its application as a chemotherapy agent to directly treat HCC [11]. Owing to the characteristics of TACE with local drug delivery, the application of ATO in TACE might attenuate the toxicity and amplify the treatment effect. ATO administration *via* cTACE shows no significant hepatic or renal toxicity and exerts a better treatment effect compared to ATO administration *via* transarterial or intravenous injection in VX2 liver tumor rabbits [12]. However, for DEB-TACE (which has the advantages of a lower systematic concentration of therapeutic drug and more persistent and stable drug delivery than cTACE), little is known about the treatment effect of ATO administration *via* DEB-TACE in patients with HCC.

In our previous study, we investigated the pharmacokinetics and intratumoral concentration of ATO-loaded CalliSpheres® microspheres (CSM) by TACE treatment in VX2 liver tumor rabbits, and we found that DEB-TACE decreased plasma, kidney and lung concentrations while increasing the intratumoral concentration of ATO without extra liver or renal toxicity compared with cTACE [13]. Our previous study suggested that ATO-loaded CSM by TACE might be a promising way to reduce systematic toxicity. Therefore, in the present study, we further investigated the effect of ATO-loaded CSM by TACE on tumor growth, angiogenesis, metastasis and survival in VX2 liver tumor rabbits, aiming to explore the antitumor property of ATO-loaded CSM by TACE in liver cancer.

Materials and methods

Animals

Healthy adult Japanese white rabbits weighing 2.8 kg~3.4 kg without sex preference or pregnancy were provided by the Experimental Animal Center of Henan Province (Henan, China). All rabbits were bred in the Laboratory Animal Center of our institution and had free access to standard diets and water during the experimental period. The study was approved by the Animal Care and Use Committee of Henan Province, and all related experiments were conducted in accordance with the principles set by the Animal Care and Use Committee of our institution.

Rabbit VX2 liver tumor model construction and validation

The rabbit VX2 liver tumor model was constructed according to the method described in a previous study [14]. The tumor location and size were measured by contrast-enhanced computed tomography (CT) at 16 d after the construction of the rabbit VX2 liver tumor model, and the tumor volume (V) was calculated according to the formula: $V = (1/2)\ ab^2$ (where a is the maximum diameter, and b is the minimum diameter). At least 120 rabbit VX2 liver tumor models were successfully constructed for the current study.

Grouping and intervention

A total of 120 VX2 liver tumor rabbits were randomly assigned into 4 groups (CSM-ATO group, cTACE-ATO group, TAE-CSM group, and control group) using the Random Number Remainder Grouping Method as described in our previous study [13]. The rabbits in the 4 groups were treated as follows: (1) CSM-ATO group: the rabbits were treated with ATO-loaded CSM (100-

300 μm, Jiangsu Hengrui Medicine Co., Ltd., China) at a dose of 0.5 mg/kg ATO and 0.1 g CSM by transcatheter arterial embolization (TAE) operation; (2) cTACE-ATO group: the rabbits were treated with a mixture of ATO and lipiodol (Laboratoire Guerbet, France) at a dose of 0.5 mg/kg ATO by TAE operation; (3) TAE-CSM group: the rabbits were treated with 0.1 g blank CSM (100-300 μm, Jiangsu Hengrui Medicine Co., Ltd., China) by TAE operation; (4) control group: the rabbits were treated with 10 ml saline by arterial injection. The detailed procedures of CSM preparation were described in our previous study [13].

TAE procedure

The VX2 liver tumor rabbits were fasted for 24 h before TAE operation. The rabbits were anesthetized by injection of Sumianxin II anesthetic (Dunhua Shengda Animal Medicine Co., Ltd., China) and then fixed on the table in the supine position. Thereafter, the right femoral artery incision area of rabbits was routinely depilated, disinfected and covered with towels. Then, the right femoral artery was exposed, and a 4F sheath (Terumo, Japan) was placed into the artery. After that, a 4F catheter (Terumo, Japan) was introduced by a guide wire, and hepatic arteriography was performed to identify the tumor supply artery and tumor site. A 2.7F coaxial microcatheter (Terumo, Japan) was catheterized to the tumor supply artery. Subsequently, ATO-loaded CSM, ATO-mixed lipiodol, blank CSM, or saline was injected into the tumor supply artery according to the grouping. For the CSM-ATO group and TAE-CSM group, the endpoint of embolism was that there was no tumor staining observed after injection; for the cTACE-ATO group, the endpoint of embolism was that no tumor staining was observed, or deposition occurred in the small branches of the portal vein. After the completion of embolism, the sheath and the catheter were removed from the artery, and the wound was sewn up.

Specimen collection/detection and survival analysis

Five VX2 liver tumor rabbits in each group were sacrificed by intravenous injection of excess sodium pentobarbital (100 mg/kg) at 12 h, 3 d, 7 d and 14 d post TAE treatment. For the survival analysis, the remaining 10 VX2 liver tumor rabbits in each group were observed until they died. Following sacrifice, the abdominal cavity of rabbits was opened to observe ascites and the tumor metastasis status, including intrahepatic metastasis, pulmonary metastasis, abdominal wall metastasis, and omentum metastasis. Tumor tissue was incised along the long axis of the primary lesion, and the total tumor volume was calculated using the formula $V = (1/2)\ ab^2$ (where a is the maximum diameter and b is the minimum diameter). Then, the tumor tissue was continuously sectioned along the long diameter at 3-5 mm intervals. One of the two pieces with the largest sectional area was photographed, fixed with 4% paraformaldehyde, dehydrated conventionally, and embedded in paraffin for further immunohistochemical (IHC) staining and the terminal deoxynucleotidyl transferase (TdT)-mediated dUTP nick end labeling (TUNEL) assay. The other piece with the largest sectional area was stored at -80°C for reverse transcription-quantitative polymerase chain reaction (RT-qPCR) assay. In addition, accumulating survival for the remaining 10 VX2 liver tumor rabbits in each group was calculated from the day of TAE treatment to the day of death.

IHC staining and analysis

IHC staining was used to assess hypoxia inducible factor-1α (HIF-1α), vascular endothelial growth factor (VEGF), matrix metalloproteinase 9 (MMP-9), twist, E-cadherin, N-cadherin, vimentin, proliferating cell nuclear antigen (PCNA) and CD31 expression in tumor tissue. The IHC staining procedures were performed in accordance with a previous study [14]. The antibodies are listed in **Table 1**. IHC staining was evaluated by two experienced pathologists in a blinded manner. All slides were examined under a light microscope throughout the entire section. HIF-1α, twist, E-cadherin, N-cadherin, vimentin and PCNA expression was determined by the percentage of positive cells in 5 high-power fields (×200) randomly selected under the microscope (Olympus Corporation, Japan) [14, 15]. VEGF and MMP-9 expression was assessed by semiquantitative IHC based on staining intensity and density [16], which was performed as follows: the staining intensity was scored as 0 (negative), 1 (weak), 2 (moderate), and 3 (strong); the staining density was scored on the basis of the percentage of positively stained cells: 0 (0%), 1 (1-25%), 2 (26-50%), 3 (51-75%), and 4 (76-100%); the total IHC score was calculated by multiplying

Table 1. Antibodies

Antibodies	Dilution ratio	Company	Country
Mouse HIF-1 alpha Monoclonal Antibody	1:50	Invitrogen	USA
Mouse VEGF Monoclonal Antibody	1:20	Invitrogen	USA
Mouse MMP9 Monoclonal Antibody	1:500	Invitrogen	USA
Rabbit CD31 Polyclonal Antibody	1:200	Bioss Inc.	USA
Rabbit Twist Polyclonal Antibody	1:200	Novus Biologicals	USA
Rabbit E-cadherin Polyclonal Antibody	1:100	MyBioSource	USA
Mouse N-cadherin Monoclonal Antibody	1:20	Invitrogen	USA
Rabbit Vimentin Polyclonal Antibody	1:500	Abcam	USA
Mouse PCNA Monoclonal Antibody	1:1000	Novus Biologicals	USA
Goat Anti-Mouse IgG H&L	1:10000	Abcam	USA
Goat Anti-Rabbit IgG H&L	1:10000	Abcam	USA

Table 2. Primers

Gene	Forward primer	Reverse primer
HIF-1α	5'-GCATCTCCGTCTCCTAACCA-3'	5'-ACACGTTAGGGCTTCTTGGA-3'
VEGF	5'-GCAGACCAAAGAAAGACAG-3'	5'-TTGCAGGAACATTTACACG-3'
Twist	5'-GGCGCTACAGTAAGAAGTCG-3'	5'-AGTCTATGTATCTGGCGGCC-3'
E-cadherin	5'-ATACCTCCCCCTTCACCGCA-3'	5'-GGATGAGCAGAGCCAGGATTC-3'
N-cadherin	5'-GCCAGGCCAAGCAACTTTTA-3'	5'-CTCTCATCCAGCCGCCGTAT-3'
Vimentin	5'-CAGGCAAAGCAGGAGTCAAAT-3'	5'-GCGAGCCATTTCTTCCTTCA-3'
β-actin	5'-TGGCTCTAACAGTCCGCCTAG-3'	5'-AGTGCGACGTGGACATCCG-3'

the intensity score by the density score, ranging from 0 to 12. CD31-positive cells were used to assess microvessel density (MVD), and any CD31-stained endothelial cell or cell cluster that was clearly separated from adjacent tissue elements was counted as a single countable microvessel [14].

TUNEL assay

Apoptotic nuclei in paraffin sections were assessed by TUNEL-DAPI kits (Roche, Germany) according to the kit instructions. Five regions were selected for each sample, and the percentage of apoptotic-positive cells in each high-power visual field (×200) was calculated for the analysis of the apoptosis rate.

RT-qPCR assay

The mRNA expression levels of HIF-1α, VEGF, twist, E-cadherin, N-cadherin, and vimentin in the tumor tissue were detected by RT-qPCR assay, which was performed as described in previous studies [14, 15, 17], and β-actin served as an internal reference. TRIzol reagent (Invitrogen, USA) was used for total RNA isolation; the First-Strand cDNA Synthesis Kit (Toyobo, Japan) was used for cDNA synthesis; SYBR Green Real-time PCR master mix (Toyobo, Japan) was used for polymerase chain reaction. The primers used in RT-qPCR are listed in **Table 2**.

Statistical analysis

Statistical analysis was performed using SPSS 24.0 software (SPSS Inc., USA) and GraphPad Prism 7.01 software (GraphPad Software Inc., USA). Data are displayed as the mean ± standard deviation or percentage. Comparisons among groups were determined by the chi-square test or multiple t test corrected using the Holm-Sidak method. Accumulating survival was displayed using the Kaplan-Meier (KM) method, and the comparison of accumulating survival between/among groups was determined by the log-rank test. A P value <0.05 was considered significant, which is displayed as $*P<0.05$, $**P<0.01$, and $***P<0.001$, while a P value >0.05 is marked as NS (not significant) in all figures.

Results

Tumor volume, metastasis site, ascites and accumulating survival

At 14 d post treatment, the tumor volume was decreased in the CSM-ATO group compared to the cTACE-ATO group ($P<0.05$), TAE-CSM group

(P<0.01) and control group (P<0.01) (**Figure 1A**). Regarding the tumor metastasis site, no difference was found in intrahepatic, pulmonary, abdominal wall, or omentum metastases between the CSM-ATO group and the cTACE-ATO group (all P>0.05); pulmonary (P<0.01), abdominal wall (P<0.01) and omentum metastases (P<0.05) were decreased in the CSM-ATO group compared to the TAE-CSM group; intrahepatic (P<0.01), pulmonary (P<0.01), abdominal wall (P<0.01) and omentum metastases (P<0.05) were decreased in the CSM-ATO group compared to the control group. Ascites were decreased in the CSM-ATO group compared to the cTACE-ATO group, TAE-CSM group and control group (all P<0.05) (**Figure 1B**). Regarding accumulating survival, it was increased in the CSM-ATO group compared to the TAE-CSM group and the control group (both P<0.01), while no difference was found between the CSM-ATO group and the cTACE-ATO group (P>0.05) (**Figure 1C**). These data indicated that ATO-loaded CSM by TACE inhibited tumor growth, metastasis and ascites while prolonging survival in VX2 liver tumor rabbits.

Tumor apoptosis and proliferation markers after treatment

Compared to the cTACE-ATO group, the tumor apoptosis rate was increased at 7 d and 14 d (both P<0.05) but was similar at 12 h and 3 d (both P>0.05) in the CSM-ATO group; moreover, it was elevated in the CSM-ATO group compared to the TAE-CSM group and control group at each time point (all P<0.05) (**Figure 2A**). For the proliferation marker, PCNA-positive cells were decreased in the CSM-ATO group compared to the cTACE-ATO group, TAE-CSM group and control group at each time point (all P<0.05) (**Figure 2B**). In addition, representative images of apoptosis detected by the TUNEL assay (peak at 12 h) and PCNA expression by IHC staining (peak at 14 d) in tumor tissue of the four groups are shown in **Figure 2C**. These data indicated that ATO-loaded CSM by TACE promoted tumor apoptosis while inhibiting proliferation in VX2 liver tumor rabbits.

HIF-1α and VEGF expression after treatment

HIF-1α mRNA expression was decreased in the CSM-ATO group compared to the cTACE-ATO group at 7 d (P<0.05) compared to the TAE-CSM group at 3 d, 7 d and 14 d (all P<0.05); however, it was increased in the CSM-ATO group compared to the control group at each time point (all P<0.001) (**Figure 3A**). HIF-1α-positive cells were also reduced in the CSM-ATO group compared to the cTACE-ATO group at 14 d and the TAE-CSM group at 7 d (both P<0.05), while they were increased in the CSM-ATO group compared to the control group at each time point (all P<0.001) (**Figure 3C**). VEGF mRNA expression was decreased in the CSM-ATO group compared to both the cTACE-ATO group and TAE-CSM group at 3 d, 7 d and 14 d (all P<0.01), while it was elevated in the CSM-ATO group compared to the control group at each time point (all P<0.001) (**Figure 3B**). Meanwhile, the VEGF IHC score was also decreased in the CSM-ATO group compared to the cTACE-ATO group and TAE-CSM group at 12 h, 3 d and 7 d (all P<0.05); however, it was increased in the CSM-ATO group compared to the control group at 12 h (P<0.01) and 3 d (P<0.001) (**Figure 3D**). In addition, representative images of HIF-1α (peak at 3 d) and VEGF (peak at 12 h) expression by IHC staining in tumor tissue of the four groups are shown in **Figure 3E**. These data suggested that ATO-loaded CSM by TACE suppressed tumor angiogenesis in VX2 liver tumor rabbits.

MVD and MMP9 expression after treatment

For MVD, no difference was found between the CSM-ATO group and cTACE-ATO group at any time point (all P>0.05); however, it was decreased in the CSM-ATO group compared to the TAE-CSM group at 3 d, 7 d and 14 d (all P<0.001), while it was increased in the CSM-ATO group compared to the control group at 7 d and 14 d (both P<0.001) (**Figure 4A**). The MMP-9 IHC score was reduced in the CSM-ATO group compared to the cTACE-ATO group, TAE-CSM group and control group at 3 d, 7 d and 14 d (all P<0.05) (**Figure 4B**). In addition, representative images of MVD (peak at 14 d) and MMP-9 (peak at 14 d) expression by IHC staining in tumor tissue of the four groups are shown in **Figure 4C**. These data further revealed that ATO-loaded CSM by TACE suppressed tumor angiogenesis and metastatic potential in VX2 liver tumor rabbits.

Epithelial-mesenchymal transition (EMT) after treatment

Twist mRNA expression was decreased in the CSM-ATO group compared to the cTACE-ATO

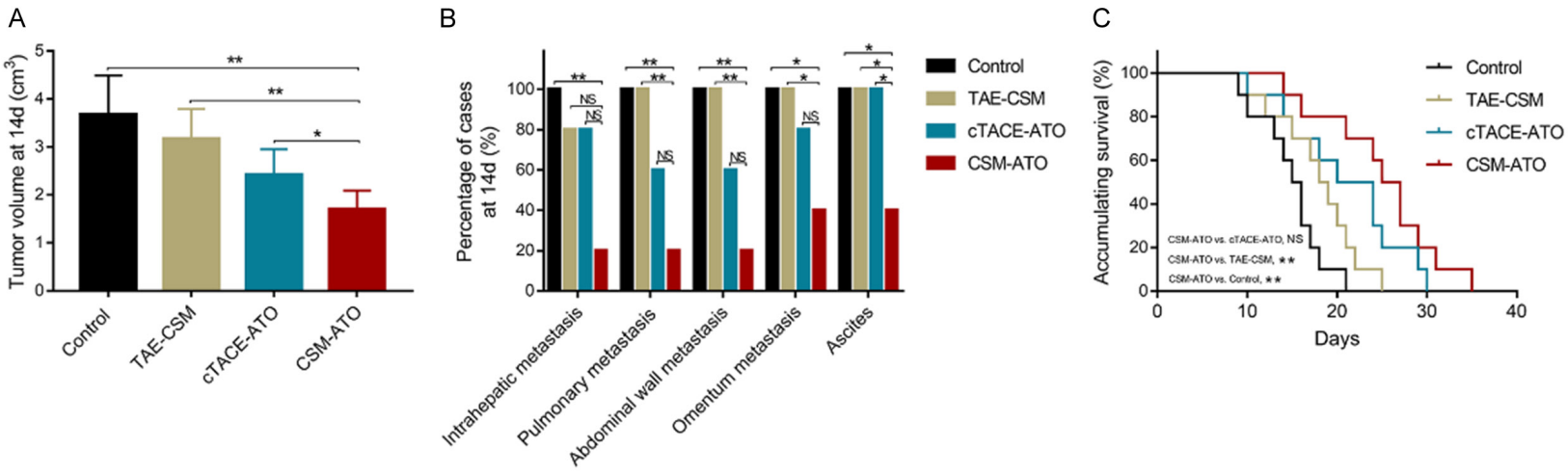

Figure 1. Comparisons of tumor volume, metastasis status, ascites, and accumulating survival among the CSM-ATO, cTACE-ATO, TAE-CSM, and control groups. A: Comparison of tumor volume in VX2 liver tumor rabbits among the CSM-ATO, cTACE-ATO, TAE-CSM, and control groups. B: Comparison of metastasis status and ascites in VX2 liver tumor rabbits among the CSM-ATO, cTACE-ATO, TAE-CSM, and control groups. C: Comparison of accumulating survival in VX2 liver tumor rabbits among the CSM-ATO, cTACE-ATO, TAE-CSM, and control groups. 14 d: 14 days; CSM: CalliSpheres® microspheres; ATO: arsenic trioxide; cTACE: conventional transarterial chemoembolization; TAE: transcatheter arterial embolization; **, $P<0.01$; *, $P<0.05$; NS, not significant.

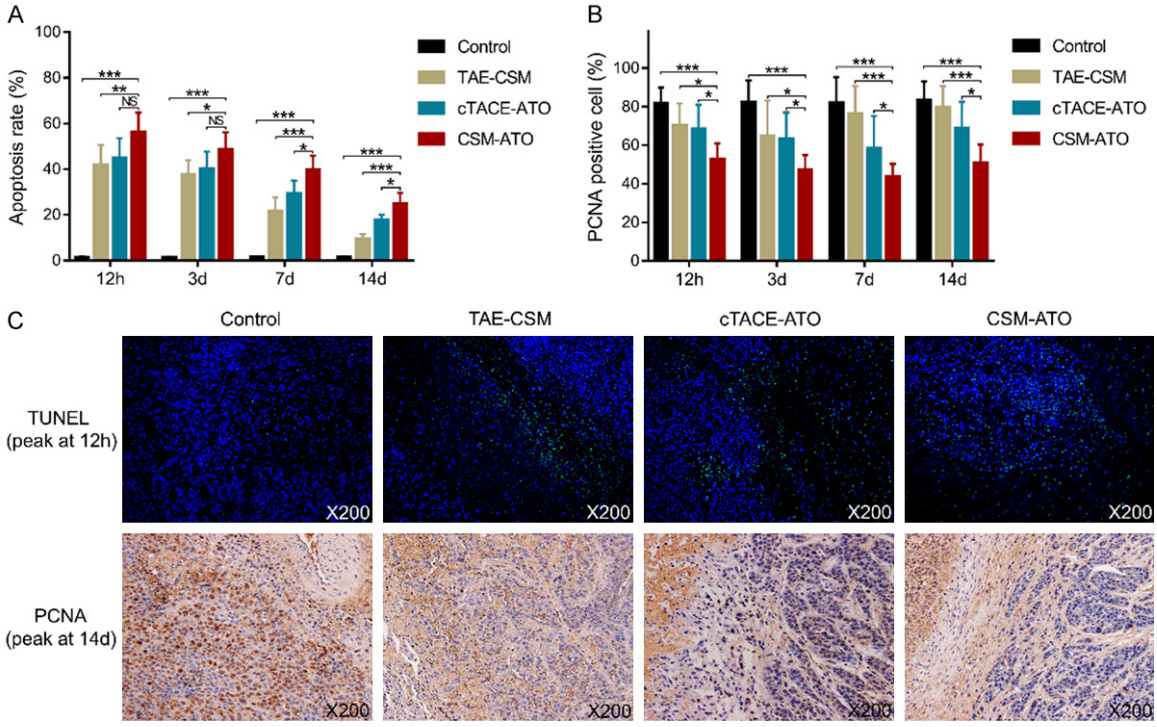

Figure 2. Comparisons of the tumor apoptosis rate and PCNA-positive cells among the CSM-ATO, cTACE-ATO, TAE-CSM, and control groups. A: Comparison of the tumor apoptosis rate in VX2 liver tumor rabbits among the CSM-ATO, cTACE-ATO, TAE-CSM, and control groups. B: Comparison of tumor PCNA-positive cells in VX2 liver tumor rabbits among the CSM-ATO, cTACE-ATO, TAE-CSM, and control groups. C: Example images of the TUNEL assay (peak at 12 h) and PCNA expression detection by IHC staining (peak at 14 d) in the four groups. 12 h: 12 hours; 3 d: 3 days; 7 d: 7 days; 14 d: 14 days; CSM: CalliSpheres® microspheres; ATO: arsenic trioxide; cTACE: conventional transarterial chemoembolization; TAE: transcatheter arterial embolization; PCNA: proliferating cell nuclear antigen; TUNEL: terminal deoxynucleotidyl transferase (TdT)-mediated dUTP nick end labeling; IHC: immunohistochemical; ***, $P<0.001$; **, $P<0.01$; *, $P<0.05$; NS, not significant.

group, TAE-CSM group and control group at 7 d and 14 d (all $P<0.05$) (**Figure 5A**). E-Cadherin mRNA expression was promoted in the CSM-ATO group compared to the cTACE-ATO group at 7 d and 14 d (both $P<0.001$); compared to the TAE-CSM group at 3 d ($P<0.05$), 7 d ($P<0.001$) and 14 d ($P<0.001$); and compared to the control group at each time point (all $P<0.05$) (**Figure 5B**). N-Cadherin mRNA expression was decreased in the CSM-ATO group compared to the cTACE-ATO group, TAE-CSM group and control group at 7 d and 14 d (all $P<0.05$) (**Figure 5C**). Vimentin mRNA expression was reduced in the CSM-ATO group compared to the cTACE-ATO group and TAE-CSM group at 7 d and 14 d (all $P<0.05$) and compared to the control group at 3 d ($P<0.05$), 7 d ($P<0.01$) and 14 d ($P<0.001$) (**Figure 5D**).

Furthermore, IHC staining was also performed. Twist-positive cells were decreased in the CSM-ATO group compared to the cTACE-ATO group at 14 d ($P<0.05$) and compared to the TAE-CSM group at 7 d and 14 d (both $P<0.05$); meanwhile, they were reduced in the CSM-ATO group compared to the control group at each time point (all $P<0.05$) (**Figure 6A**). For E-cadherin-positive cells, these were enhanced in the CSM-ATO group compared to the cTACE-ATO group and TAE-CSM group at 7 d and 14 d (all $P<0.05$); meanwhile, these cells were increased in the CSM-ATO group compared to the control group at 3 d, 7 d and 14 d (all $P<0.001$) (**Figure 6B**). For N-cadherin-positive cells as well as vimentin-positive cells, both were decreased in the CSM-ATO group compared to the TAE-CSM group and cTACE-ATO group at 7 d and 14 d (all $P<0.05$), and they were reduced in the CSM-ATO group compared to the control group at 3 d, 7 d and 14 d (all $P<0.05$) (**Figure 6C**, **6D**). In addition, representative images of twist (peak at 14 d), E-cadherin (peak at 14 d), N-cadherin (peak at 14 d) and vimentin (peak at 14 d) expression by IHC staining in tumor tissue of the four groups are shown in **Figure 6E**. These data suggested that

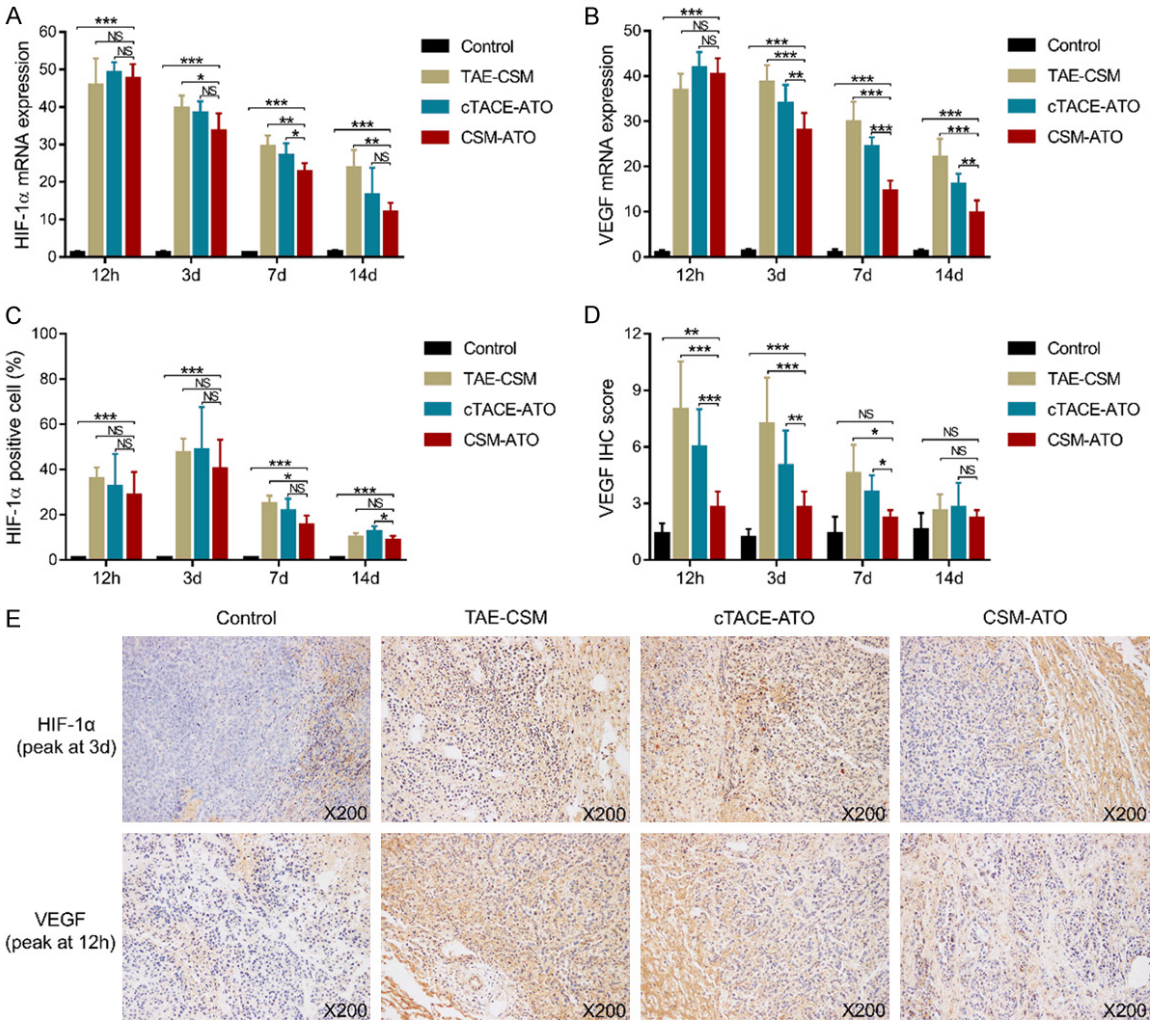

Figure 3. Comparisons of HIF-1α and VEGF among the CSM-ATO, cTACE-ATO, TAE-CSM, and control groups. A: Comparison of tumor HIF-1α mRNA expression in VX2 liver tumor rabbits among the CSM-ATO, cTACE-ATO, TAE-CSM, and control groups. B: Comparison of tumor VEGF mRNA expression in VX2 liver tumor rabbits among the CSM-ATO, cTACE-ATO, TAE-CSM, and control groups. C: Comparison of tumor HIF-1α-positive cell liver tumor rabbits among the CSM-ATO, cTACE-ATO, TAE-CSM, and control groups. D: Comparison of tumor VEGF IHC scores in VX2 liver tumor rabbits among the CSM-ATO, cTACE-ATO, TAE-CSM, and control groups. E: Example images of HIF-1α (peak at 3 d) and VEGF (peak at 12 h) expression detected by IHC staining in the four groups. 12 h: 12 hours; 3 d: 3 days; 7 d: 7 days; 14 d: 14 days; HIF-1α: hepatocyte growth factor-1α; VEGF: vascular endothelial growth factor; CSM: CalliSpheres® microspheres; ATO: arsenic trioxide; cTACE: conventional transarterial chemoembolization; TAE: transcatheter arterial embolization; IHC: immunohistochemical; ***, $P<0.001$; **, $P<0.01$; *, $P<0.05$; NS, not significant.

ATO-loaded CSM by TACE inhibited tumor EMT in VX2 liver tumor rabbits.

Illustration of CSM-ATO treatment example

At 16 d after tumor construction, the parenchymal phase of hepatic arteriography revealed a space-occupying lesion with rich blood supply in the left lateral lobe of the liver (black arrow) (Supplementary Figure 1A). After the administration of ATO-loaded CSM by TACE, hepatic arteriography revealed that the space-occupying lesion had no blood supply, indicating thorough embolism (Supplementary Figure 1B). At 1 d after treatment, the singular embolism microsphere remained round in the peritumor vessel (long arrow), and the red blood cells in the vessel gathered and formed a thrombus (short arrow). Additionally, inflammatory cell infiltration was found around the vessel. Meanwhile, peripheral liver tissue and tumor tissue (marked as T) showed extensive necrosis and bleeding (Supplementary Figure 1C). At 14 d after treatment, several embolism microsph-

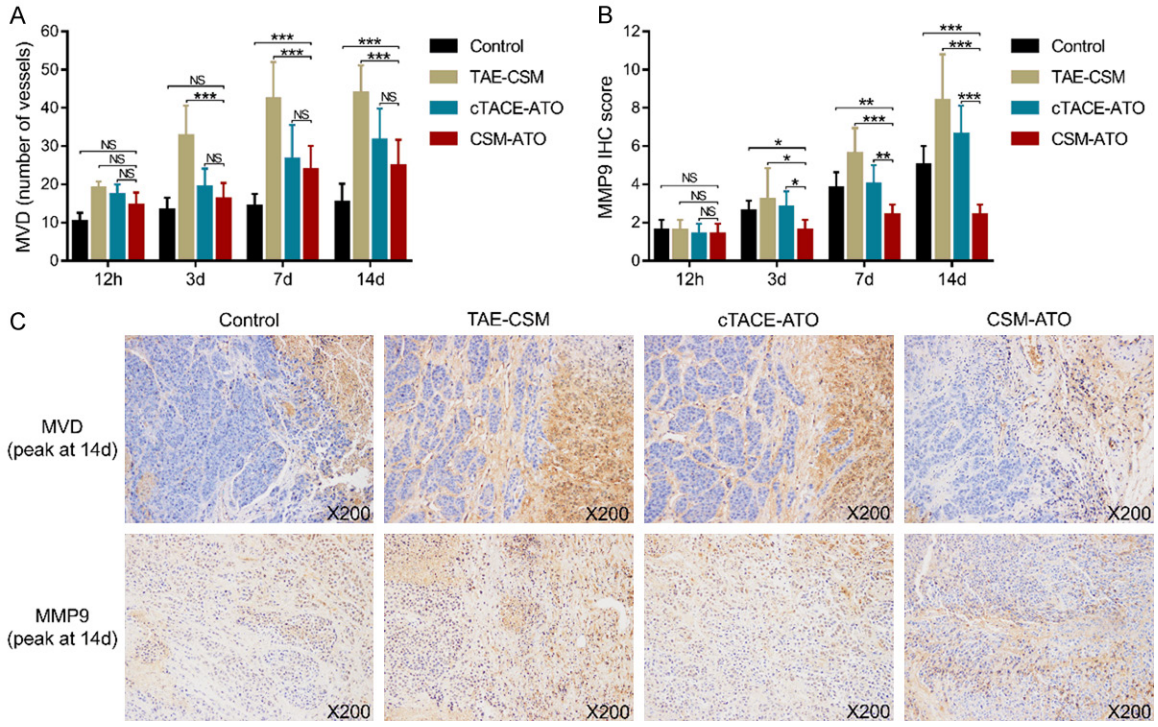

Figure 4. Comparisons of MVD and MMP-9 among the CSM-ATO, cTACE-ATO, TAE-CSM, and control groups. A: Comparisons of tumor MVD in VX2 liver tumor rabbits among the CSM-ATO, cTACE-ATO, TAE-CSM, and control groups. B: Comparisons of tumor MMP-9 in VX2 liver tumor rabbits among the CSM-ATO, cTACE-ATO, TAE-CSM, and control groups. C: Example images of MVD (marked by CD31) (peak at 14 d) and MMP-9 (peak at 14 d) expression detected by IHC staining in the four groups. 12 h: 12 hours; 3 d: 3 days; 7 d: 7 days; 14 d: 14 days; MVD: microvessel density; MMP-9: matrix metalloproteinase 9; CD31: cluster of differentiation 31; CSM: CalliSpheres® microspheres; ATO: arsenic trioxide; cTACE: conventional transarterial chemoembolization; TAE: transcatheter arterial embolization; IHC: immunohistochemical; ***, $P<0.001$; **, $P<0.01$; *, $P<0.05$; NS, not significant.

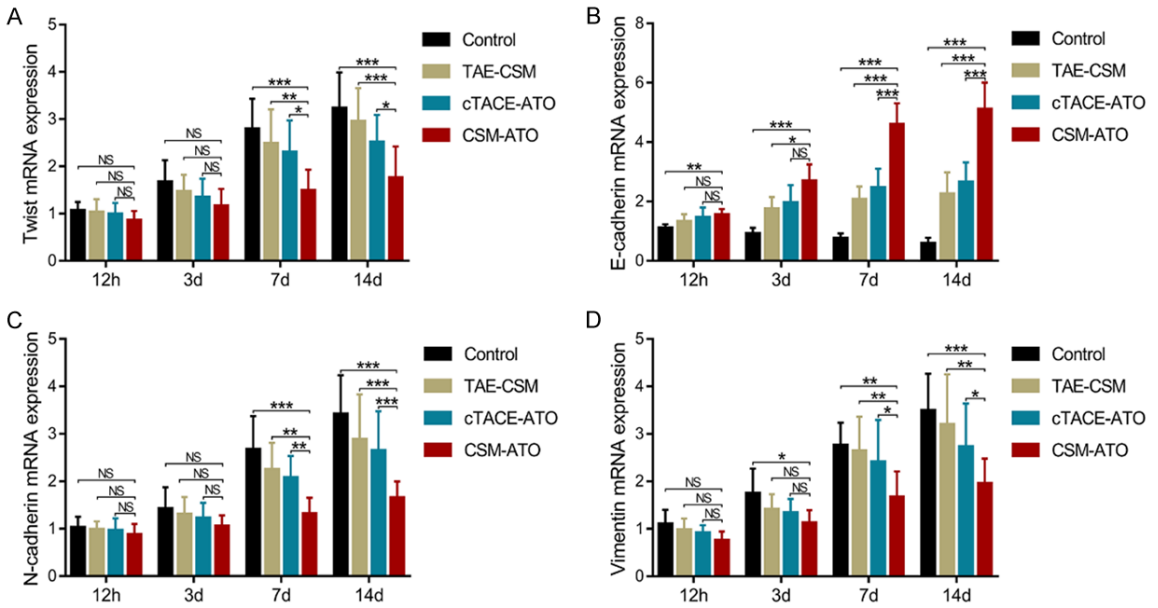

Figure 5. Comparisons of twist, E-cadherin, N-cadherin, and vimentin mRNA expression among the CSM-ATO, cTACE-ATO, TAE-CSM, and control groups. A: Comparison of tumor twist mRNA expression in VX2 liver tumor rabbits among the CSM-ATO, cTACE-ATO, TAE-CSM, and control groups. B: Comparison of tumor E-cadherin mRNA expression in VX2 liver tumor rabbits among the CSM-ATO, cTACE-ATO, TAE-CSM, and control groups. C: Comparison of tumor N-

cadherin mRNA expression in VX2 liver tumor rabbits among the CSM-ATO, cTACE-ATO, TAE-CSM, and control groups. D: Comparison of tumor vimentin mRNA expression in VX2 liver tumor rabbits among the CSM-ATO, cTACE-ATO, TAE-CSM, and control groups. 12 h: 12 hours; 3 d: 3 days; 7 d: 7 days; 14 d: 14 days; CSM: CalliSpheres® microspheres; ATO: arsenic trioxide; cTACE: conventional transarterial chemoembolization; TAE: transcatheter arterial embolization; ***, $P<0.001$; **, $P<0.01$; *, $P<0.05$; NS, not significant.

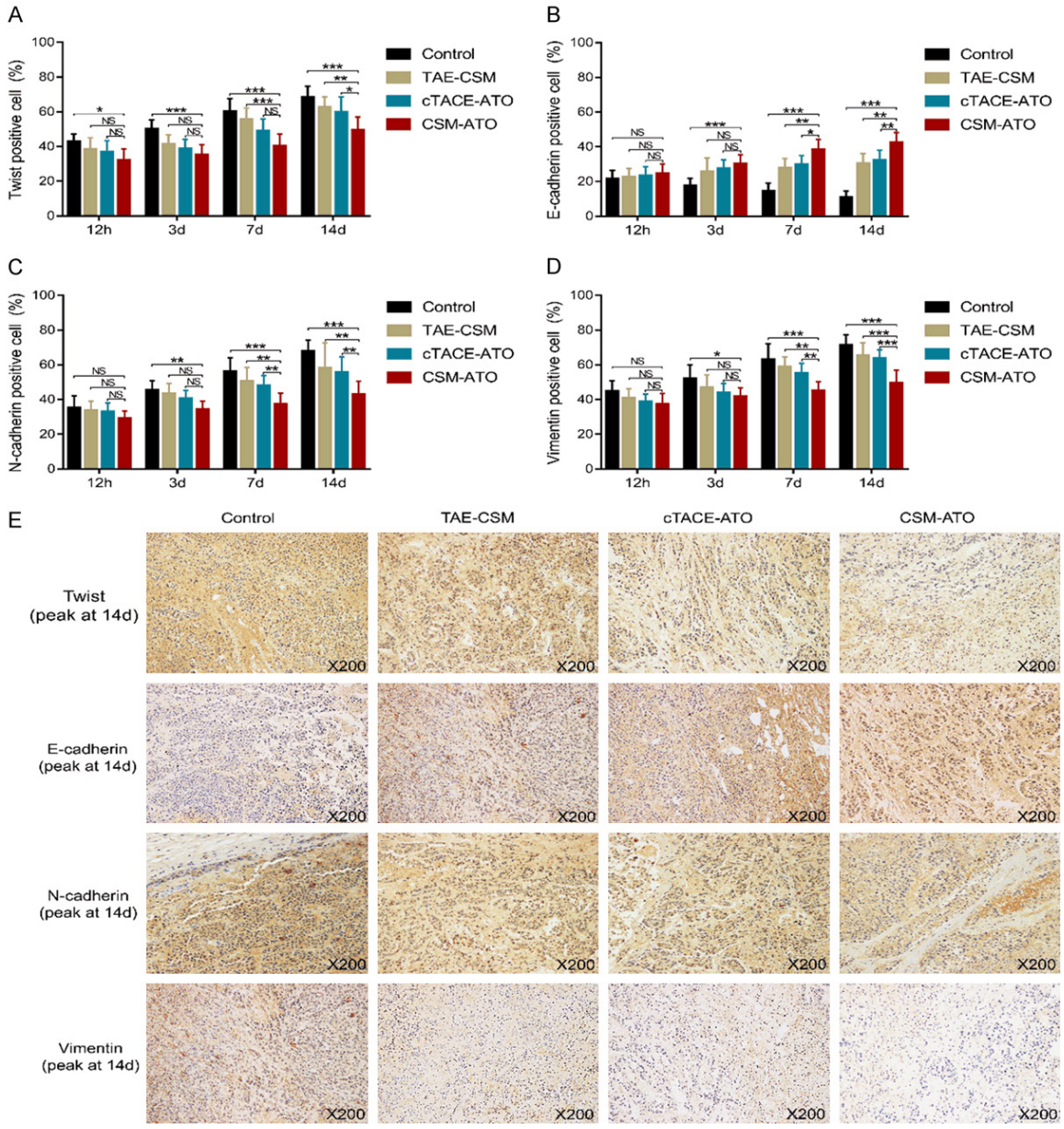

Figure 6. Comparisons of twist-, E-cadherin-, N-cadherin-, and vimentin-positive cells among the CSM-ATO, cTACE-ATO, TAE-CSM, and control groups. A: Comparison of tumor twist-positive cells in VX2 liver tumor rabbits among the CSM-ATO, cTACE-ATO, TAE-CSM, and control groups. B: Comparison of tumor E-cadherin-positive cells in VX2 liver tumor rabbits among the CSM-ATO, cTACE-ATO, TAE-CSM, and control groups. C: Comparison of tumor N-cadherin-positive cells in VX2 liver tumor rabbits among the CSM-ATO, cTACE-ATO, TAE-CSM, and control groups. D: Comparison of tumor vimentin-positive cells in VX2 liver tumor rabbits among the CSM-ATO, cTACE-ATO, TAE-CSM, and control groups. E: Example images of twist (peak at 14 d), E-cadherin (peak at 14 d), N-cadherin (peak at 14 d), and vimentin (peak at 14 d) expression detection by IHC staining in the four groups. 12 h: 12 hours; 3 d: 3 days; 7 d: 7 days; 14 d: 14 days; CSM: CalliSpheres® microspheres; ATO: arsenic trioxide; cTACE: conventional transarterial chemoembolization; TAE: transcatheter arterial embolization; IHC: immunohistochemical; ***, $P<0.001$; **, $P<0.01$; *, $P<0.05$; NS, not significant.

eres were compressed into bead bunches, and residual tumor tissue (marked as T) was found in the tumor foci (Supplementary Figure 1D). A liver specimen from a rabbit sacrificed 14 d after treatment is shown in Supplementary Figure 1E in which part of the liver presented necrosis (short arrow), and no metastatic lesion was found in the liver. The tumor tissue was cut along the largest diameter, and a small amount of peripheral tumor tissue was alive (long arrow) (Supplementary Figure 1F).

Discussion

In the present study, we investigated the treatment effect of ATO-loaded CSM by TACE in VX2 liver tumor rabbits and found that (1) ATO-loaded CSM by TACE suppressed tumor growth, metastasis, and ascites and increased accumulating survival; (2) ATO-loaded CSM by TACE repressed angiogenesis; and (3) ATO-loaded CSM by TACE inhibited EMT and metastatic potential.

TACE is listed as the first-line therapy for patients with intermediate-stage HCC and uses different drug carriers (including lipiodol (cTACE) or microspheres (DEB-TACE)) to deliver chemotherapy agents (such as doxorubicin) and exerts ischemic effects of embolization on the tumor site, resulting in a good therapeutic effect [2]. A previous study identified cTACE as an appropriate treatment with good efficacy to prolong the overall survival of patients with HCC [18]. However, the agent administered with cTACE is released abruptly, which amplifies the side effects of the therapeutic agent and further potentially limits the application of cTACE in patients with HCC, especially in fragile patients (such as Child-Pugh B patients) [19]. As one of the strategies to improve cTACE, DEB-TACE is able to release the absorbed agent more stably and persistently. According to a previous study in VX2 liver cancer rabbits, doxorubicin-loaded DEB-TACE results in vast tumor necrosis; meanwhile, a high tumor concentration but a low plasma concentration of doxorubicin is observed, and the doxorubicin level remains at its peak until 7 d after treatment [5]. Hence, DEB-TACE might possess a broader application prospective to treat HCC than cTACE.

ATO, an inorganic compound, has been used to treat diseases for 2000 years, and it has been identified to suppress the progression of HCC [20]. For instance, a recent study revealed that ATO represses the expression of cyclin B1 to induce G2/M checkpoint arrest, which further hampers the repair of damaged DNA and thus promotes apoptosis in the HCC cell line HepG2 [21]. Meanwhile, ATO inhibits VEGF mRNA and protein expression in MHCC97-H cells, and it promotes de novo ceramide synthesis to suppress MMP-9 expression in HCCLM3 cells, thereby suppressing the angiogenesis and invasion of HCC [22, 23]. Moreover, ATO downregulates twist expression in the tumor tissue of xenografted liver tumor rats and further inhibits tumor invasion as well as distant metastasis [15]. Thus, these studies indicate that ATO impairs HCC progression by inducing apoptosis while suppressing angiogenesis, invasion and metastasis. However, ATO could induce systematic toxicity, which restricts its application in treating HCC, and balancing the systematic toxicity and the treatment effect of ATO might realize its application in treating HCC. Notably, one previous study revealed that ATO administration through cTACE shows less hepatic as well as renal toxicity and enhanced treatment efficacy in VX2 liver tumor rabbits than direct ATO administration (transarterial or intravenous injection) [12]. Considering the advantage of DEB-TACE over cTACE, using CSM (which possesses high drug loading efficiency and stable release profile [24]) to load ATO and administer it by TACE might further amplify the treatment effect and lower the systematic toxicity of ATO in patients with HCC.

In our previous study, we found that ATO-loaded CSM by TACE maintained a high level of ATO in the tumor and a low level of ATO in plasma, kidney and lung by the sustained intratumoral release of ATO, and no difference was found in drug tolerance or kidney/liver impairment between ATO-loaded CSM by TACE and other treatments [13]. In this study, we further explored the effect of ATO-loaded CSM by TACE on tumor progression in VX2 liver tumor rabbits and found that ATO-loaded CSM by TACE greatly suppressed tumor growth, metastasis in multiple sites, and ascites and prolonged the accumulating survival of rabbits, which could be explained by the persistent high intratumoral level of ATO suppressing tumor growth, epithelial-mesenchymal transition (EMT)-related pathways and angiogenesis while promoting apoptosis (mentioned below) to hamper tumor growth as well as metastasis, which further resulted in prolonged survival of

VX2 liver tumor rabbits. In addition, we discovered that ATO-loaded CSM by TACE inhibited proliferation while promoting apoptosis in tumors. A possible explanation might be that the persistent high intratumoral concentration of ATO induced cell cycle arrest, impeded DNA repair and promoted apoptosis to suppress the proliferation of HCC cells [21]. However, the effect of ATO-loaded CSM by TACE on cell proliferation should be further verified by KI67 detection in tumor tissues, and drug toxicity should also be investigated. In this study, we only used CSM to evaluate ATO administration by DEB-TACE, and further studies using microspheres from different brands could be investigated.

HIF-1α and VEGF are two vital regulators that promote angiogenesis in solid tumors including HCC [19]. After cTACE treatment, HIF-1α expression has been reported to be upregulated by hypoxia in residual tumor tissue; moreover, it increases VEGF expression to enhance angiogenesis and accelerate the progression of residual tumors, eventually boosting recovery or even metastasis of tumor lesions [25]. In the present study, the data showed that ATO-loaded CSM by TACE increased HIF-1α and VEGF expression as well as MVD in VX2 liver tumor rabbits, which could be explained by hypoxia in tumors after treatment increasing HIF-1α, thus enhancing VEGF expression and further promoting angiogenesis [19]. In addition, we also found that ATO-loaded CSM by TACE had less effect on promoting HIF-1α and VEGF expression as well as MVD than cTACE. A possible explanation might be that the persistent high level of ATO in tumors attenuated the increase in HIF-1α and VEGF expression caused by hypoxia, which further suppressed angiogenesis and thus reduced MVD in tumor tissue after treatment [22].

EMT is a critical biological process that participates in the regulation of migration and invasion of HCC [26]. Among the regulators of EMT, the transition of cadherin is also vital in which the transition of E-cadherin towards N-cadherin induces the acquisition of a fibroblast-like phenotype in tumor cells and further promotes their invasiveness and metastasis ability [27]. Moreover, Twist and its downstream target vimentin participate in the regulation of several key signaling pathways, including EMT, to promote the progression of cancers [28, 29]. In this study, we found that ATO-loaded CSM by TACE decreased N-cadherin, twist and vimentin expression while increasing E-cadherin expression in the tumor tissues of VX2 liver tumor rabbits, which could be explained by the following: (1) the sustained high level of ATO inhibited the phosphorylation of STAT3 to promote E-cadherin while suppressing N-cadherin expression [30]; and (2) the persistent high level of ATO in tumors suppressed the activity of twist, which further decreased vimentin expression. In addition, ATO-loaded CSM by TACE also suppressed MMP-9 expression, which further illustrated the inhibitory effect of ATO-loaded CSM by TACE on metastasis.

To the best of our knowledge, this study was the first to evaluate the treatment effect of ATO-loaded CSM by TACE in liver tumor-bearing animals; however, several issues in this study should be clarified. First, according to previous studies, the dose of ATO varies from 0.5-5 mg/kg in a liver tumor rabbit model [12, 13]. We chose the dose of ATO at 0.5 mg/kg for the following two reasons: (1) the drug-loaded microspheres used in this study presented with good embolization effect; thus, a lower dose of ATO was more appropriate for this study; and (2) considering the safety of experimental animals, the dose of the chemotherapeutic agent should be minimized under the premise of acquiring reliable data; therefore, we finally chose 0.5 mg/kg ATO after performing a preliminary experiment (data not shown). Second, the literature and standards on evaluating the prognosis of tumor-bearing animals after DEB-TACE treatment were relatively limited; thus, we chose the tumor volume at 14 d after treatment to evaluate the effect of different therapies on tumor progression. Further studies verifying our results in other tumor-bearing animal models and determining the effect of ATO-loaded CSM by TACE on signaling pathways are encouraged.

To conclude, ATO-loaded CSM by TACE exerts good antitumor effects, as shown by the decrease in tumor growth, angiogenesis, and metastasis and the prolongation of the accumulating survival in VX2 liver tumor rabbits, which indicates that ATO-loaded CSM by TACE might be a potential therapy for HCC. However, more studies are needed to further validate this conclusion.

Acknowledgements

This study was supported by the National Natural Science Foundation of China (No. 81401-494) and the Henan Province Medical Science and Technology Project (No. 201403059).

Disclosure of conflict of interest

None.

Address correspondence to: Xinwei Han and Jianzhuang Ren, Department of Interventional Radiology, The First Affiliated Hospital, Zhengzhou University, No. 1 East Jianshe Road, Zhengzhou 450052, P. R. China. Tel: +86-0371-66278081; Fax: +86-0371-66278082; E-mail: aoxin00807@126.com (XWH); jimo98714818547@126.com (JZR)

References

[1] Bray F, Ferlay J, Soerjomataram I, Siegel RL, Torre LA and Jemal A. Global cancer statistics 2018: GLOBOCAN estimates of incidence and mortality worldwide for 36 cancers in 185 countries. CA Cancer J Clin 2018; 68: 394-424.

[2] European Association for the Study of the Liver. Electronic address: easloffice@easloffice.eu; European Association for the Study of the Liver. EASL clinical practice guidelines: management of hepatocellular carcinoma. J Hepatol 2018; 69: 182-236.

[3] Raoul JL, Sangro B, Forner A, Mazzaferro V, Piscaglia F, Bolondi L and Lencioni R. Evolving strategies for the management of intermediate-stage hepatocellular carcinoma: available evidence and expert opinion on the use of transarterial chemoembolization. Cancer Treat Rev 2011; 37: 212-220.

[4] Lammer J, Malagari K, Vogl T, Pilleul F, Denys A, Watkinson A, Pitton M, Sergent G, Pfammatter T, Terraz S, Benhamou Y, Avajon Y, Gruenberger T, Pomoni M, Langenberger H, Schuchmann M, Dumortier J, Mueller C, Chevallier P and Lencioni R; PRECISION V Investigators. Prospective randomized study of doxorubicin-eluting-bead embolization in the treatment of hepatocellular carcinoma: results of the PRECISION V study. Cardiovasc Intervent Radiol 2010; 33: 41-52.

[5] Hong K, Khwaja A, Liapi E, Torbenson MS, Georgiades CS and Geschwind JF. New intra-arterial drug delivery system for the treatment of liver cancer: preclinical assessment in a rabbit model of liver cancer. Clin Cancer Res 2006; 12: 2563-2567.

[6] Zou JH, Zhang L, Ren ZG and Ye SL. Efficacy and safety of cTACE versus DEB-TACE in patients with hepatocellular carcinoma: a meta-analysis. J Dig Dis 2016; 17: 510-517.

[7] Oki E, Ando K, Nakanishi R, Sugiyama M, Nakashima Y, Kubo N, Kudou K, Saeki H, Nozoe T, Emi Y and Maehara Y. Recent advances in treatment for colorectal liver metastasis. Ann Gastroenterol Surg 2018; 2: 167-175.

[8] Antman KH. Introduction: the history of arsenic trioxide in cancer therapy. Oncologist 2001; 6 Suppl 2: 1-2.

[9] Wang HY, Zhang B, Zhou JN, Wang DX, Xu YC, Zeng Q, Jia YL, Xi JF, Nan X, He LJ, Yue W and Pei XT. Arsenic trioxide inhibits liver cancer stem cells and metastasis by targeting SRF/MCM7 complex. Cell Death Dis 2019; 10: 453.

[10] Shen L, Zhang G, Lou Z, Xu G and Zhang G. Cryptotanshinone enhances the effect of Arsenic trioxide in treating liver cancer cell by inducing apoptosis through downregulating phosphorylated-STAT3 in vitro and in vivo. BMC Complement Altern Med 2017; 17: 106.

[11] Lin CC, Hsu C, Hsu CH, Hsu WL, Cheng AL and Yang CH. Arsenic trioxide in patients with hepatocellular carcinoma: a phase II trial. Invest New Drugs 2007; 25: 77-84.

[12] Fu X, Luo RG, Qiu W, Ouyang L, Fan GQ, Liang QR and Tang Q. Sustained release of arsenic trioxide benefits interventional therapy on rabbit VX2 liver tumor. Nanomedicine 2020; 24: 102118.

[13] Duan XH, Li H, Ren JZ, Han XW, Chen PF, Li FY, Huang GH and Ju SG. Hepatic arterial chemoembolization with arsenic trioxide eluting callispheres microspheres versus lipiodol emulsion: pharmacokinetics and intratumoral concentration in a rabbit liver tumor model. Cancer Manag Res 2019; 11: 9979-9988.

[14] Liang B, Zheng CS, Feng GS, Wu HP, Wang Y, Zhao H, Qian J and Liang HM. Correlation of hypoxia-inducible factor 1alpha with angiogenesis in liver tumors after transcatheter arterial embolization in an animal model. Cardiovasc Intervent Radiol 2010; 33: 806-812.

[15] Wang GZ, Zhang W, Fang ZT, Zhang W, Yang MJ, Yang GW, Li S, Zhu L, Wang LL, Zhang WS, Liu R, Qian S, Wang JH and Qu XD. Arsenic trioxide: marked suppression of tumor metastasis potential by inhibiting the transcription factor Twist in vivo and in vitro. J Cancer Res Clin Oncol 2014; 140: 1125-1136.

[16] Hu Z, Gu X, Zhong R and Zhong H. Tumor-infiltrating CD45RO(+) memory cells correlate with favorable prognosis in patients with lung adenocarcinoma. J Thorac Dis 2018; 10: 2089-2099.

[17] Moussa M, Goldberg SN, Kumar G, Sawant RR, Levchenko T, Torchilin V and Ahmed M. Radiofrequency ablation-induced upregulation of hypoxia-inducible factor-1alpha can be suppressed with adjuvant bortezomib or liposo-

mal chemotherapy. J Vasc Interv Radiol 2014; 25: 1972-1982.
[18] Lencioni R, de Baere T, Soulen MC, Rilling WS and Geschwind JF. Lipiodol transarterial chemoembolization for hepatocellular carcinoma: asystematic review of efficacy and safety data. Hepatology 2016; 64: 106-116.
[19] Gaba RC, Emmadi R, Parvinian A and Casadaban LC. Correlation of doxorubicin delivery and tumor necrosis after drug-eluting bead transarterial chemoembolization of rabbit VX2 liver tumors. Radiology 2016; 280: 752-761.
[20] Marelli L, Stigliano R, Triantos C, Senzolo M, Cholongitas E, Davies N, Tibballs J, Meyer T, Patch DW and Burroughs AK. Transarterial therapy for hepatocellular carcinoma: which technique is more effective? A systematic review of cohort and randomized studies. Cardiovasc Intervent Radiol 2007; 30: 6-25.
[21] Luo Q, Li Y, Deng J and Zhang Z. PARP-1 inhibitor sensitizes arsenic trioxide in hepatocellular carcinoma cells via abrogation of G2/M checkpoint and suppression of DNA damage repair. Chem Biol Interact 2015; 226: 12-22.
[22] Cui L, Gao B, Cao Z, Chen X, Zhang S and Zhang W. Downregulation of B7-H4 in the MHCC97-H hepatocellular carcinoma cell line by arsenic trioxide. Mol Med Rep 2016; 13: 2032-2038.
[23] Zhang S, Zhou J, Zhang C, Wu H, Wang Y, Bian J, Guo J and Wu X. Arsenic trioxide inhibits HCCLM3 cells invasion through de novo ceramide synthesis and sphingomyelinase-induced ceramide production. Med Oncol 2012; 29: 2251-2260.
[24] Xiang H, Long L, Yao Y, Fang Z, Zhang Z and Zhang Y. CalliSpheres drug-eluting bead transcatheter arterial chemoembolization presents with better efficacy and equal safety compared to conventional TACE in treating patients with hepatocellular carcinoma. Technol Cancer Res Treat 2019; 18: 1533033819830751.
[25] Shim JH, Park JW, Kim JH, An M, Kong SY, Nam BH, Choi JI, Kim HB, Lee WJ and Kim CM. Association between increment of serum VEGF level and prognosis after transcatheter arterial chemoembolization in hepatocellular carcinoma patients. Cancer Sci 2008; 99: 2037-2044.
[26] Giannelli G, Koudelkova P, Dituri F and Mikulits W. Role of epithelial to mesenchymal transition in hepatocellular carcinoma. J Hepatol 2016; 65: 798-808.
[27] Panebianco C, Saracino C and Pazienza V. Epithelial-mesenchymal transition: molecular pathways of hepatitis viruses-induced hepatocellular carcinoma progression. Tumour Biol 2014; 35: 7307-7315.
[28] Yang J, Mani SA, Donaher JL, Ramaswamy S, Itzykson RA, Come C, Savagner P, Gitelman I, Richardson A and Weinberg RA. Twist, a master regulator of morphogenesis, plays an essential role in tumor metastasis. Cell 2004; 117: 927-939.
[29] Meng J, Chen S, Han JX, Qian B, Wang XR, Zhong WL, Qin Y, Zhang H, Gao WF, Lei YY, Yang W, Yang L, Zhang C, Liu HJ, Liu YR, Zhou HG, Sun T and Yang C. Twist1 regulates vimentin through Cul2 circular RNA to promote EMT in hepatocellular carcinoma. Cancer Res 2018; 78: 4150-4162.
[30] Huang Y, Zhou B, Luo H, Mao J, Huang Y, Zhang K, Mei C, Yan Y, Jin H, Gao J, Su Z, Pang P, Li D and Shan H. ZnAs@SiO2 nanoparticles as a potential anti-tumor drug for targeting stemness and epithelial-mesenchymal transition in hepatocellular carcinoma via SHP-1/JAK2/STAT3 signaling. Theranostics 2019; 9: 4391-4408.

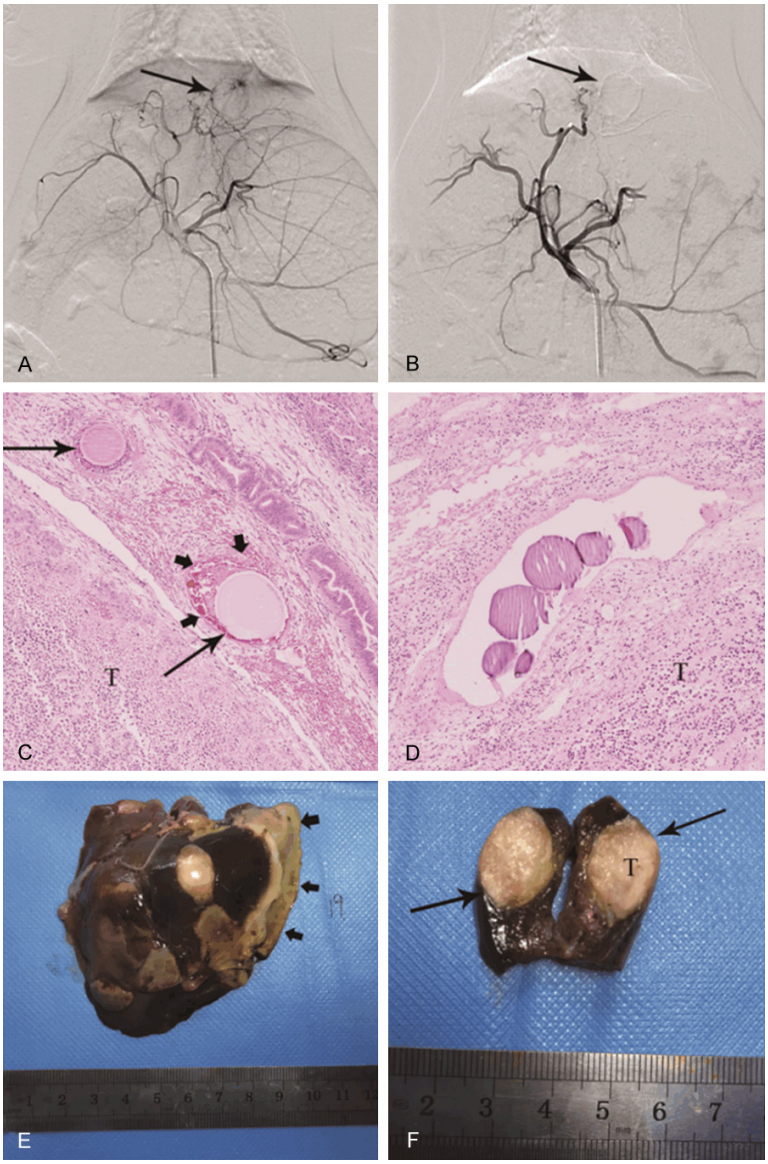

Supplementary Figure 1. Representative images of CSM-ATO treatment. A: The parenchymal phase of hepatic arteriography of tumors in VX2 liver tumor rabbits at 16 d after tumor construction. B: The parenchymal phase of hepatic arteriography of tumors in VX2 liver tumor rabbits after treatment. C: The morphology of CSM beads in the peritumor vessels of VX2 liver tumor rabbits at 1 d after treatment. D: The morphology of CSM beads in the peritumor vessels of VX2 liver tumor rabbits at 14 d after treatment. E: The liver specimens of VX2 liver tumor rabbits at 14 d after treatment. F: Tumor specimens (cut by the maximum diameter) of VX2 liver tumor rabbits at 14 d after treatment. CSM: CalliSpheres® microspheres; ATO: arsenic trioxide; T: tumor tissue.